JOURNAL OF GEOPHYSICAL RESEARCH, VOL. 113, C01020, doi:10.1029/2007JC004402, 2008

Click Here for Full Article

Kuril Islands tsunami of November 2006: 1. Impact at Crescent City by distant scattering

Z. Kowalik,[1] J. Horrillo,[1] W. Knight,[2] and Tom Logan[3]

Received 18 June 2007; revised 30 August 2007; accepted 2 November 2007; published 31 January 2008.

[1] A numerical model for the global tsunami computation constructed by Kowalik et al. (2005, 2007a) is applied to the tsunami of November 15, 2006 in the northern Pacific with spatial resolution of one minute. Numerical results are compared to sea level data collected by Pacific DART buoys. The tide gauge at Crescent City (CC) recorded an initial tsunami wave of about 20 cm amplitude and a second larger energy packet arriving 2 hours later. The first energy input into the CC harbor was the primary (direct) wave traveling over the deep waters of the North Pacific. Interactions with submarine ridges and numerous seamounts located in the tsunami path were a larger source of tsunami energy than the direct wave. Travel time for these amplified energy fluxes is longer than for the direct wave. Prime sources for the larger fluxes at CC are interactions with Koko Guyot and Hess Rise. Tsunami waves travel next over the Mendocino Escarpment where the tsunami energy flux is concentrated owing to refraction and directed toward CC. Local tsunami amplification over the shelf break and shelf are important as well. In many locations along the North Pacific coast, the first arriving signal or forerunner has lower amplitude than the main signal, which often is delayed. Understanding this temporal distribution is important for an application to tsunami warning and prediction. As a tsunami hazard mitigation tool, we propose that along with the sea level records (which are often quite noisy), an energy flux for prediction of the delayed tsunami signals be used.

Citation: Kowalik, Z., J. Horrillo, W. Knight, and T. Logan (2008), Kuril Islands tsunami of November 2006: 1. Impact at Crescent City by distant scattering, *J. Geophys. Res.*, *113*, C01020, doi:10.1029/2007JC004402.

1. Introduction

[2] On 15 November 2006 at 11:14:16 (UTC) an earthquake with moment magnitude 8.3 (http://earthquake.usgs.gov/eqcenter/recenteqsww/Quakes/usvcam.php) generated a tsunami near the Kuril Islands. Tsunamis propagated over the entire Pacific Ocean. The resulting sea level disturbance was recorded by DART buoys located in the open ocean and by many coastal tide gauges. Buoy data showed that the duration of tsunami signal while propagating away from the source was steadily increasing (with distance from source) and that often the first group of tsunami waves did not include the highest waves. Along the Japanese coast, the highest tsunami waves arrived just minutes after the initial tsunami waves arrival (largest amplitude 40 cm occurred at Hanasaki). The initial wave at Kahului (Maui) of 50 cm amplitude was followed 2 hours later by a wave of 76 cm amplitude. This pattern can be observed in many locations along the Pacific coast. The small initial tsunami of about 20 cm was barely noticed at Crescent City (CC). The highest wave of about 88 cm amplitude was recorded 2–3 hours later. No other west coast tidal stations recorded such a high wave. Large tsunamis which propagate globally can be amplified in locations remote from the source zone. The Chile (1960) and Alaska (1964) earthquakes generated tsunamis which produced unusually high waves in many distant locations. The 1960 tsunami, well recorded along the US West Coast, produced amplitudes often in excess of 1 m with the largest wave height of 1.7 m measured at CC [*Lander and Lockridge*, 1989]. The tsunami from the Alaska Good Friday earthquake (1964) generated wave amplitudes in excess of 1 m along the U.S. West Coast. Again CC suffered the greatest damage owing to a high wave exceeding 4 m amplitude [*Wiegel*, 1965]. Using the Kuril tsunami example we intend to investigate the behavior of the transoceanic tsunami and the special conditions which cause tsunami enhancement at CC. Our investigation is aimed to demonstrate that the tsunami amplification at CC is caused by both the redirection of tsunami energy over long distances of propagation and by amplification due to the local bathymetry. The effects of amplifications of the distant tsunami were studied by *Hebert et al.* [2001] by examining tsunami inundations observed on the Marquesas Islands. One case study considered by *Hebert et al.* [2001] was the 1994 Kuril tsunami. It clearly demonstrated the importance of long volcanic ridges and fracture zones in directing tsunami signal toward the distant locations and it

[1]Institute of Marine Science, University of Alaska Fairbanks, Fairbanks, Alaska, USA.
[2]West Coast and Alaska Tsunami Warning Center, Palmer, Alaska, USA.
[3]Arctic Region Supercomputing Center, University of Alaska Fairbanks, Fairbanks, Alaska, USA.

Copyright 2008 by the American Geophysical Union.
0148-0227/08/2007JC004402$09.00

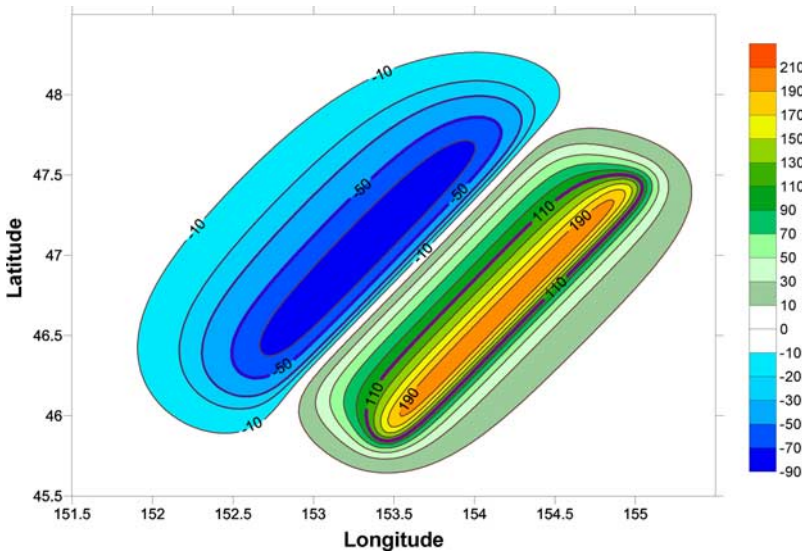

Figure 1. Source function (bottom deformation in centimeters) for the tsunami of 15 November 2006.

bears strong resemblance to the 15 November 2006 tsunami. Studies of topographic transformations of tsunami signal in the open ocean due to ridges were summarized by *Mei et al.* [2005]. Usually, incident energy flux on a ridge is split into reflected and transmitted fluxes. The scattering of tsunami energy by bottom topography in such an approach is a function of depth of water over topographic features. In order to better understand this process, *Mofjeld et al.* [2000] introduced a tsunami scattering index which is expressed by the ratio of the transmitted wave amplitude to that of the incident wave. One cannot exclude the possibility of a more complicated process like resonant interaction of the tsunami wave and ridge bathymetry. *Snodgrass et al.* [1962] demonstrated the presence of discrete spectra in waves trapped over depth discontinuities and *Mei et al.* [2005] showed that over a stepped bottom ridge the discrete spectra exist as well. If an incident wave can excite these trapped modes, an amplification of the tsunami signal due to resonance will follow. The high-resolution model applied to the Indian Ocean Tsunami of 2004 [*Kowalik et al.*, 2005, 2007a] showed a complex pattern of tsunami/bathymetry interaction. In the southern Pacific, and especially the Atlantic Ocean, tsunami wave propagation was accompanied by wave energy ducting along oceanic ridges. Travel time for these amplified energy fluxes was much longer than the travel time of the first wave. Therefore the arrival time of these amplified waves is important for tsunami warning and prediction.

[3] Amplification of the tsunami signal at CC during the events of 1960 and 1964 was investigated by assuming distant or local enhancement. *Mader and Bernard* [1993] and *Bernard et al.* [1994] modeled the Aleutian Island (Unimak Island) tsunami of April 1946 and the March 1964 tsunami generated in the Gulf of Alaska, concluding that directionality of the tsunami source was the primary cause of the tsunami enhancement. On the other hand the amplification was frequently studied assuming that either local (harbor) geometry or shelf and coastal geometry has natural periods in the tsunami range of periods [*Roberts and Kauper*, 1964; *Keulegan et al.*, 1969]. The interaction of the tsunami wave with the shelf geometry often results in the trapping and amplification of the tsunami energy. *Gonzalez et al.* [1995] suggested that the high-amplitude tsunami waves generated by the 25 April 1992 Cape Mendocino earthquake at CC were induced by the coastal trapped edge wave. An analytical solution of tsunamis obliquely incident on a continental slope derived by *Koshimura et al.* [1999] confirms existence of the amplification of the edge waves and possibility of a resonance in the period range of tsunamis. New observations of tsunamis at the coast of Japan by *Yanuma and Tsuji* [1998] indicate that the shelf trapped edge wave strongly interact with the fundamental mode of a nearby harbor.

2. Source Function

[4] The generation mechanism for the Kuril Islands tsunami model is the static sea floor uplift caused by abrupt slip at the plate interface. Actual sea floor uplift has a complicated structure composed of many blocks motion [*Lobkovsky et al.*, 2006] but often it is considered as one continuous block [*Okada*, 1985]. Permanent, vertical sea floor displacement is computed using the static dislocation formulae from *Okada* [1985]. Inputs to these formulae are parameters defining the fault plane geometry: depth (13 km), strike (215°), dip (15°), slip (92°), length (240 km), and width (80 km) as well as seismic moment (Mo = 3.5×10^{28} dyne cm) and rigidity (4.2×10^{11}dyne cm^{-2}). The bottom displacement used in computation is given in a rectangular region 45°N–49°N and 152°E–156°E; see Figure 1.

3. Distribution of Maximum Amplitude

[5] To study tsunamis, the vertically averaged equations of motion and continuity are formulated in spherical polar coordinates [*Gill*, 1982]. Dissipation is described by the nonlinear bottom friction term with nondimensional coefficient $r = 0.003$. The solution of this set of equations is advanced in time by the two-time-level numerical scheme.

For the spatial derivatives the second order of approximation is constructed [*Imamura*, 1996; *Mader*, 2004; *Kowalik et al.*, 2005, 2007a]. The full description of the numerical model is given by *Kowalik et al.* [2005]. A special numerical scheme is developed for the nonlinear terms in the equations of motion and continuity on the basis of the higher-order upwind-downwind approach. The spatial grid step of numerical computation was 1 arcminute and the time step was set to 2 s. The total number of grid points was close to 100 million. A small spatial step is important as the short-period waves can be obliterated during large distances of propagation when using larger spatial steps. The integration domain extends from 80°S to 69°N and from 120°E to 70°W. The boundaries include both wet and dry points. At coastal (dry points) the normal velocity is set to zero. New dry and wet points may be generated through the runup/rundown) algorithm. At wet points on domain boundaries, the radiation condition established by *Reid and Bodine* [1968] is used. Model computations using the tsunami source (Figure 1) were made for 20 hours of propagation, allowing the tsunami signal to cross the entire Pacific Ocean. During computation the maximum tsunami amplitude in every grid point was recorded. The plot of maximum amplitude in the Pacific Ocean is shown in Figure 2.

[6] The maximum amplitude distribution in Figure 2 shows that the tsunami traveled over the entire Pacific. The elongated tsunami source (Figure 1) directs the main lobe of wave energy toward the southern hemisphere, but strong maximum amplitudes are also observed along the shores of the North Pacific. Some of the tsunami energy propagates in a finger-like pattern, a product of wave refraction and focusing around islands/seamounts/passages chain systems. Closer examinations show that the oceanic ridges and seamounts tend to refocus tsunami energy. Our interest is in energy concentration along the Mendocino Escarpment which is directed toward Crescent City. Figure 2 also depicts the amplitude enhancement in shallow water region along the coasts and especially around the islands. Even islands located far from the source such as the Galapagos or Marquesas show quite strong tsunami amplification due to coastal energy trapping.

4. Important Stages in the Kuril Islands Tsunami Development

[7] Although tsunami spreads over the entire Pacific, the main signal was confined to the northern hemisphere. In this domain we intend to investigate tsunami development and especially tsunami amplification in the vicinity of Crescent City (CC). The tsunami onset was registered on 15 November 2006 at 11:14:16(UTC). The starting time in all our computations ($t = 0$) is the tsunami onset time. The model results will be compared with data recorded by DART buoys. In Figure 3 the bathymetry used in our computation (based on work by *British Oceanographic Data Centre* [2003]) and some locations of DART buoys are given.

[8] Bathymetric features important in reorganizing and focusing tsunami signal toward CC are shown in Figure 3. Tsunami propagation is shown in Figure 4. The signal as generated by the source from the Figure 1 is traveling as a positive wave toward the southeast Pacific and as a negative wave into Okhotsk Sea (Figure 4, top plot). While interacting with the Emperor Seamount Chain and with the exceptionally large Koko Guyot [*Davies et al.*, 1972] tsunami is scattered into new directions and by interference generates a new set of waves (Figure 4, second plot). Further tsunami energy is trapped and dispersed by the Hess Rise (Figure 4, third plot).

[9] A complicated packet of waves arrives at CC, with the first arrival preserving the properties of the initial wave generated in the Kuril Islands trench, and a second, larger wave group arriving about 2 hours later. Differences in the wave front direction show that the two waves travel different routes. While the first wave group arrives from the northwest via the great circle route and deep Aleutian trench, the second wave group arrives from the west. This latter wave is directed toward CC by secondary sources. The comparison of the tsunami signal recorded by DART buoys and calculated by the model are given in Figure 5.

[10] The overall amplitude recorded at DART buoy locations is of the order of a few centimeters. These are typical tsunami amplitudes for buoys anchored in deep oceanic basins far from the source zone and off the main energy lobe. The computation simulates relatively well the first cycle of wave motion and the amplitude modulation in time in all buoys. Computations for the DART buoy closest to CC (D411, located at 127°W, 39.34°N) turned out to be in satisfactory agreement with recorded sea level. To investigate tsunami signal enhancement by the Mendocino Escarpment (i.e., step-like bathymetry change) three time-series numerical results are shown in Figure 6. The numerical gauges are located along 127°W longitude at 43°20′N, 41°20′N and 39°20′N, respectively. The deeper numerical gauge is situated south of the Mendocino Escarpment at a depth of 4304 m. The other two are situated north of the Mendocino Escarpment (on the step). One is facing CC (middle gauge) at a depth of 2585 m and the other just north at a depth of 2948 m.

[11] The first wave arrivals are quite similar at all numerical gauges and they show an increasing time delay going from north to south. Thus we can conclude that the first tsunami signal arrives from the north or northwest. The largest amplitude in the second packet of waves arrives about 2 hours after the initial tsunami, and peaks at about 2.7 cm at the northern numerical gauge, 4.7 cm at the middle gauge, and 2 cm at the southern gauge.

5. Why Tsunami is Amplified Along the Mendocino Escarpment: Energy Flux Approach

[12] Observations of the Kuril Islands tsunami in Crescent City (CC) showed that the initial wave of 15–25 cm amplitude was followed about 2 hours later by a wave of 60–80 cm amplitude. Inspection of the DART buoy D411 (127°W, 39.34°N, in Figure 5) which is closest to CC, show that the sea level variations two hours after the initial wave are only slightly amplified when compared to the initial wave. It seems that amplification shown in Figure 2 takes place in the very narrow range of latitudes. To study the energy from the distant tsunami sources it is natural to introduce the energy flux vector [*Kowalik et al.*, 2007b]. In the rectangular system of coordinates, with the x coordinate along E-W direction and y along N-S direction, the

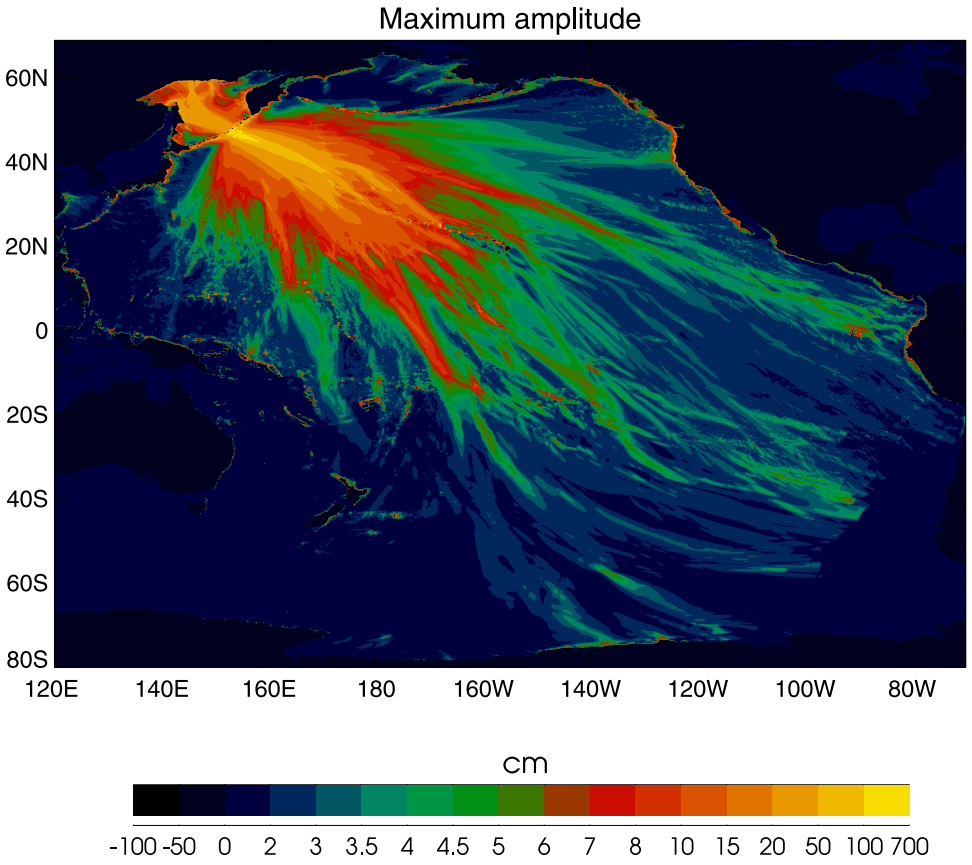

Figure 2. Maximum modeled tsunami amplitude in the Pacific.

u component of velocity along x direction can be combined with the sea level (ζ) to define the E-W component of the energy flux vector [e.g., *Kowalik and Murty*, 1993],

$$E_x = \rho H u\left[g\zeta + \frac{1}{2}\left(u^2 + v^2\right)\right]. \quad (1)$$

[13] Similarly, the N-S component of the energy flux vector is defined (with v, the velocity component along the y direction),

$$E_y = \rho H v\left[g\zeta + \frac{1}{2}\left(u^2 + v^2\right)\right], \quad (2)$$

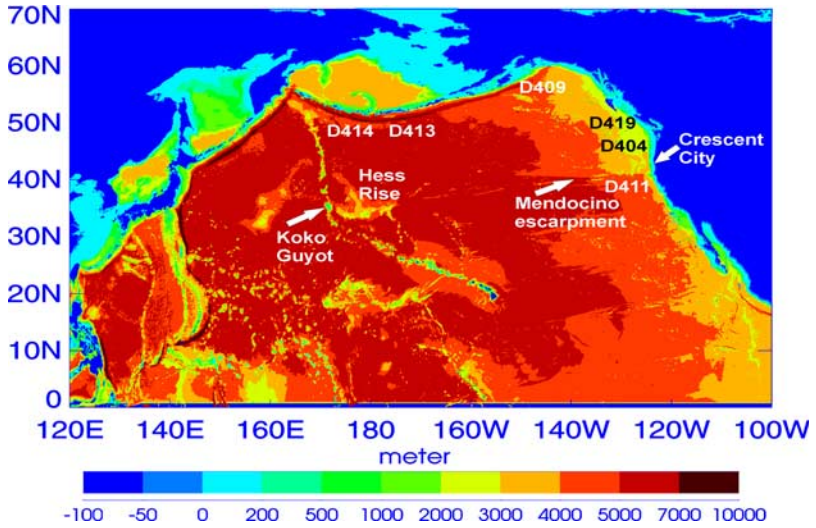

Figure 3. One-minute resolution bathymetry based on the GEBCO Atlas [*British Oceanographic Data Centre*, 2003]. Shown are DART buoys used in comparison with model.